Cold elastic and reactive atom-molecule collisions in helium–helium–alkali-metal triatomic systems

Hiroya Suno*
RIKEN Advanced Institute for Computational Science, Kobe 650-0047, Japan
and RIKEN Nishina Center for Accelerator-Based Science, Wako 351-0198, Japan

B. D. Esry
Department of Physics, Kansas State University, Manhattan, Kansas 66506, USA
(Received 12 March 2014; published 6 May 2014)

Atom-molecule collisions in helium–helium–alkali-metal triatomic systems at cold energies are studied using the adiabatic hyperspherical representation. We consider the elastic collision processes $^4\mathrm{He}X + {}^4\mathrm{He} \rightarrow {}^4\mathrm{He}X + {}^4\mathrm{He}$ and $^4\mathrm{He}_2 + X \rightarrow {}^4\mathrm{He}_2 + X$, as well as the reactive collision processes $^4\mathrm{He}X + {}^4\mathrm{He} \rightleftharpoons {}^4\mathrm{He}_2 + X$, where X is one of the bosonic alkali-metal atoms: ^{7}Li, ^{23}Na, ^{39}K, ^{85}Rb, or ^{133}Cs. The elastic and reactive collision cross sections are calculated at nonzero collision energies by including not only zero atom-molecule relative angular momentum, $L = 0$, processes but also $L > 0$ processes. The total cross section for $^4\mathrm{He}X + {}^4\mathrm{He} \rightarrow {}^4\mathrm{He}X + {}^4\mathrm{He}$ is found to increase with the scattering length between ^{4}He and X, while the other collision processes are not found to have any systematic dependence on the alkali-metal species X.

DOI: 10.1103/PhysRevA.89.052701 PACS number(s): 34.50.Cx, 34.10.+x

I. INTRODUCTION

Three-body collision processes have been attracting considerable interest due to their relevance for the rapidly growing field of cold and ultracold atomic gases [1,2]. In such systems, elastic, inelastic, and reactive atom-molecule collisions are of great interest, in addition to three-body recombination and collision-induced dissociation. Elastic atom-molecule collisions are crucial for determining the dynamics of ultracold atom-molecule mixtures at the mean-field level, while inelastic and reactive atom-molecule collisions have a large impact on the lifetime of Feshbach molecules in such mixtures [3–5]. Furthermore, in the regime of large two-body s-wave scattering length a, achieved near a Feshbach resonance [6–8], three-body collision processes exhibit universal scaling behavior with a as a result of Efimov physics [9–14]. These universal aspects have been observed experimentally in recent years [15–21] and confirm our understanding of three-body universal properties [2,14].

When ultracold three-body collisions become universal, the dynamics are then predominantly determined by the long-range behavior of the atom-atom scattering wave function, and the complicated atom-atom interaction can therefore be replaced with a simple model that is designed to reproduce the same long-range behavior. It is in this context that the adiabatic hyperspherical representation has been applied frequently to the calculations on three-body collisions. While the use of a model interaction allows us to get deeper insights into three-body collision processes, carrying out such calculations for chemically important species using realistic interactions would require substantial further technical development.

However, there exist a few realistic systems simple enough to be treated within the adiabatic hyperspherical representation. So far, triatomic helium systems, for which there exists only one dimer bound state with zero orbital angular momentum $l = 0$, have been studied within the adiabatic hyperspherical representation by us [22,23]. Wang *et al.* [24] have recently treated cold three-body collision processes and bound states in spin-stretched H–H–alkali-metal systems, for which, again, there exists only one diatomic bound state. We have also studied cold three-body recombination and bound states in ^{4}He–^{4}He–alkali-metal systems [25,26], which have one ^{4}He–alkali-metal and one ^{4}He-^{4}He bound state. These results are relevant to the buffer gas cooling technique used in cold and ultracold gas experiments [27–29]. Extension to the more complicated Ne-Ne-H system, for which there exist several diatomic bound states with $l \geqslant 0$, has been carried out by Parker *et al.* [30] using the "diabatic-by-sectors" approach. A more recent development by Wang *et al.* [31] has permitted the inclusion of hundreds of channels in a recombination calculation for model potentials but has not yet been applied to realistic interactions.

In this paper, we study elastic and reactive atom-molecule collisions involving two helium atoms and one alkali-metal atom at cold collision energies. This work extends the previous investigations in Refs. [25,26], which dealt with three-body recombination and bound states in the same triatomic systems. We calculate the cross sections for the elastic collision processes

$$\begin{aligned} {}^4\mathrm{He}X + {}^4\mathrm{He} &\rightarrow {}^4\mathrm{He}X + {}^4\mathrm{He} \quad \text{and} \\ {}^4\mathrm{He}_2 + X &\rightarrow {}^4\mathrm{He}_2 + X, \end{aligned} \tag{1}$$

as well as the reactive collision processes

$$ {}^4\mathrm{He}X + {}^4\mathrm{He} \rightleftharpoons {}^4\mathrm{He}_2 + X, \tag{2}$$

where X is one of the bosonic alkali-metal atoms: ^{7}Li, ^{23}Na, ^{39}K, ^{87}Rb, or ^{133}Cs. We consider not only zero atom-molecular relative angular momentum, $L = 0$, processes but also $L > 0$ processes. We use the helium dimer interaction potential of Jeziorska *et al.* [32] and the KTTY helium–alkali-metal potential of Kleinekathöfer *et al.* [33]. The key ingredient

*suno@riken.jp

in our numerical calculations is the adiabatic hyperspherical representation [22,34,35]. A modified version of Whitten and Smith's democratic hyperspherical coordinate system [22,36] is combined with specific boundary conditions to impose the permutation symmetry of the two bosonic ^{4}He atoms. The R-matrix method [37,38] is then used to obtain the scattering S matrix, which allows us to obtain the cross sections for elastic and reactive atom-molecule collisions.

This paper is organized as follows. We explain our method and give all necessary formulas for calculating the cross sections for atom-molecule collisions in Sec. II. The results are presented and discussed in Sec. III. A summary of this work is given in Sec. IV. We use atomic units throughout except where explicitly stated otherwise.

II. THEORETICAL METHOD

We solve the Schrödinger equation for three interacting atoms using the adiabatic hyperspherical representation [22,34,35]. In the adiabatic hyperspherical representation, we calculate eigenfunctions and eigenvalues of the fixed-hyperradius Hamiltonian in order to construct a set of coupled-channel hyperradial equations. The R-matrix method [37,38] is then used to extract the scattering matrix from these coupled equations. The method employed has been detailed elsewhere [22,23], but we include a brief description here for completeness and clarity.

After the usual separation of the center-of-mass motion, the three-body system is described by six coordinates. For these coordinates, we use a modified version of Whitten-Smith's democratic hyperspherical coordinates $(R,\Omega) \equiv (R,\theta,\varphi,\alpha,\beta,\gamma)$ [22,36]. The hyperradius R describes the global size of the three-particle system, while the Euler angles (α,β,γ) specify the orientation of the body-fixed frame in space. The two hyperangles (θ,φ) describe the shape of the molecular triangle. In terms of a rescaled wave function $\psi_E = R^{5/2}\Psi_E$, with Ψ_E being the usual solution, the nuclear Schrödinger equation for three particles interacting through the potential $V(R,\theta,\varphi)$ is written as

$$\left[-\frac{1}{2\mu}\frac{\partial^2}{\partial R^2} + \frac{\Lambda^2+15/4}{2\mu R^2} + V(R,\theta,\varphi)\right]\psi_E(R,\Omega) = E\psi_E(R,\Omega), \tag{3}$$

where Λ^2 is the squared "grand canonical angular momentum operator" [22,39,40] and μ is the three-body reduced mass given by

$$\mu^2 = \frac{m_1 m_2 m_3}{m_1+m_2+m_3}, \tag{4}$$

with m_i $(i = 1,2,3)$ being the masses of particle i. In our convention, we designate the alkali-metal atom particle 1 and the ^{4}He atomsparticles 2 and 3.

The interaction potential $V(R,\theta,\varphi)$ used in this work is expressed as the sum of three two-body terms,

$$V(R,\theta,\varphi) = v_{\mathrm{He}X}(r_{12}) + v_{\mathrm{HeHe}}(r_{23}) + v_{\mathrm{He}X}(r_{31}), \tag{5}$$

where r_{ij} are the interparticle distances. For the helium dimer potential $v_{\mathrm{HeHe}}(r)$, we use the representation of Jeziorska *et al.* [32]; and for the helium–alkali-metal potentials $v_{\mathrm{He}X}(r)$, the KTTY representation of Kleinekathöfer *et al.* [33]. Each of these two-body potentials is found to support only one bound state. Our interaction potential in Eq. (5) includes neither retardation nor nonadditive three-body terms. Based on our experience in Ref. [23] and the weak polarizability of the helium atoms, we do not expect the three-body term to contribute significantly, but retardation may have a substantial effect on the calculated cross sections. To our knowledge, retardation corrections for the HeX systems are not available. The ^{4}He$_2$ and ^{4}HeX bound-state energies $E_{v=0,l=0}$ and the scattering lengths a calculated with these two-body interaction potentials, taken from Refs. [25,26], are summarized in Table I.

TABLE I. ^{4}He$_2$ and ^{4}HeX bound-state energy E_{00} (1 a.u. = $3.157\,746\,5 \times 10^8$ mK) and scattering lengths a calculated using the two-body potentials from Refs. [32,33].

System	E_{00} (a.u.)	E_{00} (mK)	a (a.u.)	a (Å)
^{4}He$_2$	-5.472×10^{-9}	-1.728	165.4	87.53
^{4}He^{7}Li	-1.780×10^{-8}	-5.622	92.29	48.84
^{4}He^{23}Na	-9.178×10^{-8}	-28.98	44.14	23.36
^{4}He^{39}K	-3.547×10^{-8}	-11.20	62.96	33.32
^{4}He^{85}Rb	-3.253×10^{-8}	-10.27	64.27	34.01
^{4}He^{133}Cs	-1.566×10^{-8}	-4.945	85.63	45.31

The first step is to solve the fixed-R adiabatic eigenvalue equation for a given set of quantum numbers J (total nuclear orbital angular momentum), M (its projection on a laboratory-fixed axis), and Π (parity with respect to the inversion of the nuclear coordinates),

$$\left[\frac{\Lambda^2+15/4}{2\mu R^2} + V(R,\theta,\varphi)\right]\Phi_\nu(R;\Omega) = U_\nu(R)\Phi_\nu(R;\Omega), \tag{6}$$

to obtain the channel functions $\Phi_\nu(R;\Omega)$ and the potential curves $U_\nu(R)$. The above adiabatic equation, (6), is solved by expanding the channel functions on Wigner rotation matrices

$$\Phi_\nu^{JM\Pi}(R;\Omega) = \sum_K \phi_{K\nu}^{J\Pi}(R;\theta,\varphi) D_{KM}^J(\alpha,\beta,\gamma), \tag{7}$$

where K is the projection of the total nuclear orbital angular momentum on a body-fixed axis and takes the values $K = J, J-2, \ldots, -(J-2), -J$ for the parity-favored case, $\Pi = (-1)^J$, and $K = J-1, J-3, -(J-3), -(J-1)$ for the parity-unfavored case, $\Pi = (-1)^{J+1}$. The remaining degrees of freedom (θ,φ) are solved by expansion onto a direct product of fifth-order basis splines [41] in θ and φ. The hyperangles (θ,φ) span, respectively, the ranges $[0,\pi/2]$ and $[0,2\pi]$. But, for φ, due to the identical particle symmetry of the two ^{4}He atoms, we only need to consider the range $\varphi \in [0,\pi]$ with the following boundary conditions at $\varphi = 0$,

$$(-1)^{J+K}\phi_{-K,\nu}(R;\theta,0) = \phi_{K\nu}(R;\theta,0), \tag{8}$$

$$(-1)^{J+K+1}\left.\frac{\partial\phi_{-K,\nu}}{\partial\varphi}\right|_{\varphi=0} = \left.\frac{\partial\phi_{K\nu}}{\partial\varphi}\right|_{\varphi=0}, \tag{9}$$

and at $\varphi = \pi$,

$$(-1)^J \phi_{-K,\nu}(R;\theta,\pi) = \phi_{K\nu}(R;\theta,\pi), \tag{10}$$

$$(-1)^{J+1} \frac{\partial \phi_{-K,\nu}}{\partial \varphi}\bigg|_{\varphi=\pi} = \frac{\partial \phi_{K\nu}}{\partial \varphi}\bigg|_{\varphi=\pi}. \tag{11}$$

We generate the basis splines for θ with 100 mesh points, while we use 120 mesh points for φ. A uniform mesh can be employed for small hyperradii R, while for large R the mesh should be dense around the two-body coalescence points at $(\theta,\varphi) = (\pi/2, \pi - 2\arctan(m_2/\mu))$ and $(\pi/2,\pi)$, where the potential surface $V(R,\theta,\varphi)$ changes abruptly.

The adiabatic eigenfunction expansion gives the total wave function ψ_E in terms of the complete, orthonormal set of angular wave functions Φ_ν and radial wave functions $F_{\nu E}$,

$$\psi_E(R,\Omega) = \sum_\nu F_{\nu E}(R)\Phi_\nu(R;\Omega), \tag{12}$$

where ν is a collective index that includes all the quantum numbers necessary to identify each channel. If the expansion in Eq. (12) includes the complete, infinite set of Φ_ν, this representation of ψ_E is exact. In practice, the sum is truncated to a finite number of terms but can be extended systematically to obtain any desired level of accuracy. Insertion of ψ_E from Eq. (12) into the Schrödinger equation from Eq. (3) results in a set of coupled ordinary differential equations,

$$\left[-\frac{1}{2\mu}\frac{d^2}{dR^2} + U_\nu(R)\right]F_{\nu E}(R) - \frac{1}{2\mu}\sum_{\nu'}\left[P_{\nu\nu'}(R)\frac{d}{dR} + \frac{d}{dR}P_{\nu\nu'}(R) + Q_{\nu\nu'}(R)\right]F_{\nu' E}(R) = E F_{\nu E}(R), \tag{13}$$

where the nonadiabatic coupling elements are given by

$$P_{\nu\nu'}(R) = \left\langle\!\left\langle \Phi_\nu \left| \frac{d}{dR} \right| \Phi_{\nu'} \right\rangle\!\right\rangle, \tag{14}$$

$$Q_{\nu\nu'}(R) = -\left\langle\!\left\langle \frac{d\Phi_\nu}{dR} \middle| \frac{d\Phi_{\nu'}}{dR} \right\rangle\!\right\rangle. \tag{15}$$

The double-bracket matrix element signifies that integrations are carried out only over the angular coordinates Ω.

In practice, we solve Eq. (6) for a set of about 200 radial grid points R_i up to $R \approx 2000$ a.u. in order to obtain the potential curves $U_\nu(R)$ and the coupling matrix elements $P_{\nu\nu'}(R)$ and $Q_{\nu\nu'}(R)$. For $R > 2000$ a.u., they are extrapolated using their known asymptotic forms [38]. We solve Eq. (13) using the finite-element method [38]. About 10^4 elements, in each of which fifth-order polynomials are used to expand the radial wave function, extend from $R = 8$ to $R = 5 \times 10^5$ a.u., and 12 adiabatic channels are included. These are sufficient to obtain the results accurate to two significant digits. The scattering S matrix is then extracted using the R-matrix method [37].

III. RESULTS AND DISCUSSION

Since both the $^4He_2$ and the ^{4}He–alkali-metal molecules have only a single $l = 0$ bound state, atom-molecule collisions are allowed only for the parity-favored case, $\Pi = (-1)^J$, and the atom-molecule relative angular momentum L should equal the three-body total angular momentum J. We can therefore limit ourselves only to $J^\Pi = 0^+, 1^-, 2^+$, etc. For each of these symmetries, the lowest adiabatic hyperspherical potential curve $\nu = 0$ corresponds to the ^{4}HeX + ^{4}He channel, that is, a ^{4}He–alkali-metal molecule with one ^{4}He atom far away in the limit $R \to \infty$. This potential curve asymptotically behaves as

$$U_0(R) - \frac{1}{2\mu}Q_{00}(R) \to E_{00}^{^4\mathrm{He}X} + \frac{J(J+1)}{2\mu R^2} \quad \text{for} \quad R \to \infty, \tag{16}$$

where $E_{00}^{^4\mathrm{He}X}$ is the energy of the ^{4}HeX molecule. The second-lowest potential curve $\nu = 1$ corresponds to the $^4He_2 + X$ channel and asymptotically behaves as

$$U_1(R) - \frac{1}{2\mu}Q_{11}(R) \to E_{00}^{^4\mathrm{He}^4\mathrm{He}} + \frac{J(J+1)}{2\mu R^2} \quad \text{for} \quad R \to \infty, \tag{17}$$

where $E_{00}^{^4\mathrm{He}^4\mathrm{He}}$ is the energy of the ^{4}He dimer. All higher potential curves, $\nu = 2,3,\ldots$, correspond to the three-body continuum channels, i.e., all three atoms far away from each other in the limit $R \to \infty$. These potential curves behave as

$$U_\nu(R) \to \frac{\lambda(\lambda+4) + 15/4}{2\mu R^2} \quad \text{for} \quad R \to \infty. \tag{18}$$

In principle, λ can take on any non-negative integer value, but its possible values are restricted by the requirements of permutation symmetry. All these potential curves were obtained in our previous investigations in Refs. [25,26], and the other details of the potential curves are explained in those publications. Here, as an illustration, we only show the potential curves $U_\nu(R)$ for the ^{4}He-^{4}He-^{39}K system in the $J^\Pi = 1^-$ symmetry in Fig. 1.

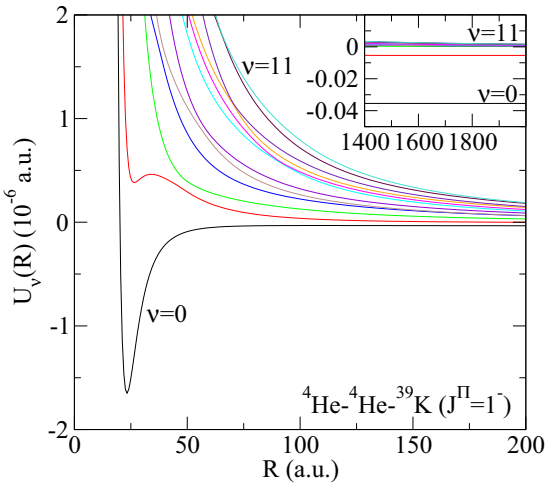

FIG. 1. (Color online) The 12 lowest adiabatic hyperspherical potential curves $U_\nu(R)$ (ν = 0–11) for the ^{4}He-^{4}He-^{39}K system in the $J^\Pi = 1^-$ symmetry. The lowest, $\nu = 0$, and second-lowest, $\nu = 1$, potential curves represent the atom-molecule channels corresponding asymptotically to ^{4}He^{39}K + ^{4}He and $^4He_2$ + ^{39}K, respectively. The higher channels, ν = 2–11, represent the three-body continuum channels. Inset: Threshold-energy region at large hyperradii.

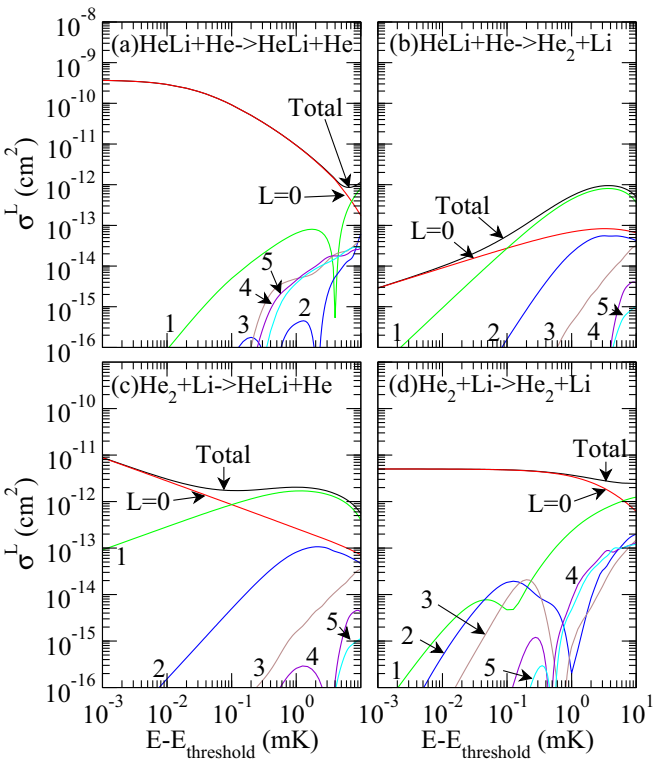

FIG. 2. (Color online) Total and partial cross sections for elastic and reactive atom-molecule collisions involving the ^{4}He-^{4}He-^{7}Li system. We show cross sections for (a) $^4\mathrm{He}^7\mathrm{Li} + {}^4\mathrm{He} \to {}^4\mathrm{He}^7\mathrm{Li} + {}^4\mathrm{He}$, (b) $^4\mathrm{He}^7\mathrm{Li} + {}^4\mathrm{He} \to {}^4\mathrm{He}_2 + {}^7\mathrm{Li}$, (c) $^4\mathrm{He}_2 + {}^7\mathrm{Li} \to {}^4\mathrm{He}^7\mathrm{Li} + {}^4\mathrm{He}$, and (d) $^4\mathrm{He}_2 + {}^7\mathrm{Li} \to {}^4\mathrm{He}_2 + {}^7\mathrm{Li}$.

In terms of the scattering S-matrix elements, the atom-molecule collision cross section from channel i to channel f is expressed as

$$\sigma_{f\leftarrow i} = \sum_L \sigma^L_{f\leftarrow i} = \sum_L \frac{(2L+1)\pi}{k_i^2} \left| S^{J=L,\Pi=(-1)^L}_{f\leftarrow i} - \delta_{fi} \right|^2, \tag{19}$$

where $\sigma^L_{f\leftarrow i}$ is the partial atom-molecule collision cross section corresponding to the relative angular momentum L, $k_i = [2\mu_i(E - E_i)]^{1/2}$ is the atom-molecule wave number associated with the initial channel i, and μ_i and E_i are, respectively, the atom-molecule reduced mass and the energy of the molecule. In our case, we have $\mu_0 = m_{^4\mathrm{He}}(m_{^4\mathrm{He}} + m_X)/(2m_{^4\mathrm{He}} + m_X)$ and $E_0 = E_{00}^{^4\mathrm{He}X}$ for the $v = 0$ channel corresponding to $^4\mathrm{He}X + {}^4\mathrm{He}$ and $\mu_1 = 2m_{^4\mathrm{He}}m_X/(2m_{^4\mathrm{He}} + m_X)$ and $E_1 = E_{00}^{^4\mathrm{He}^4\mathrm{He}}$ for the $v = 1$ channel corresponding to $^4\mathrm{He}_2 + X$.

Figures 2(a)–2(d) show the total and partial cross sections for elastic and reactive atom-molecule collisions involving the ^{4}He-^{4}He-^{7}Li system. The cross sections for the elastic $^4\mathrm{He}^7\mathrm{Li} + {}^4\mathrm{He}$ collision are shown in Fig. 2(a); those for the reactive process $^4\mathrm{He}^7\mathrm{Li} + {}^4\mathrm{He} \to {}^4\mathrm{He}_2 + {}^7\mathrm{Li}$, in Fig. 2(b); those for the process $^4\mathrm{He}_2 + {}^7\mathrm{Li} \to {}^4\mathrm{He}^7\mathrm{Li} + {}^4\mathrm{He}$, in Fig. 2(c); and those for the elastic $^4\mathrm{He}_2 + {}^7\mathrm{Li}$ collision, in Fig. 2(d). The partial cross sections corresponding to atom-molecule relative angular momenta from $L = 0$ to $L = 5$ are included in the total cross section. The cross sections are plotted as functions of the energy with respect to the threshold in each process, that is, $E_{\mathrm{threshold}} = E_{\max(i,f)}$. For the elastic $^4\mathrm{He}^7\mathrm{Li} + {}^4\mathrm{He}$ collision in Fig. 2(a), the $L = 0$ partial cross section dominates for collision energies below about 5 mK, above which the $L = 1$ partial-wave contribution becomes dominant. The other $L = 2$–5 partial cross sections are mostly negligible and may contribute only near 10 mK. The total cross section is converged to two digits with respect to the number of angular momenta L and, thus, can be considered the definitive total cross section, unless the $L \geqslant 6$ partial cross sections are unexpectedly large. We recall that their threshold behavior is determined solely by L and follows the Wigner threshold law $\sigma^L_{0\leftarrow 0} \sim (E - E_{00}^{^4\mathrm{He}^7\mathrm{Li}})^{2L}$. For the reactive collision process $^4\mathrm{He}^7\mathrm{Li} + {}^4\mathrm{He} \to {}^4\mathrm{He}_2 + {}^7\mathrm{Li}$ in Fig. 2(b), only the $L = 0$ and 1 partial cross sections contribute, and the other partial cross sections are negligible for the collision energies considered here. The convergence of the total cross section is thus more certain. The threshold behavior follows $\sigma^L_{1\leftarrow 0} \sim (E - E_{00}^{^4\mathrm{He}^4\mathrm{He}})^{L+1/2}$. For the process $^4\mathrm{He}_2 + {}^7\mathrm{Li} \to {}^4\mathrm{He}^7\mathrm{Li} + {}^4\mathrm{He}$ in Fig. 2(c), too, only the $L = 0$ and 1 partial cross sections contribute, with the other angular momenta being negligible, and the total cross section can be considered to be converged. The threshold behavior is given by $\sigma^L_{0\leftarrow 1} \sim (E - E_{00}^{^4\mathrm{He}^4\mathrm{He}})^{L-1/2}$. Finally, for the elastic $^4\mathrm{He}_2 + {}^7\mathrm{Li}$ collision in Fig. 2(d), the $L = 0$ partial cross section dominates below about 5 mK, beyond which the $L = 1$ partial cross section becomes dominant. At higher

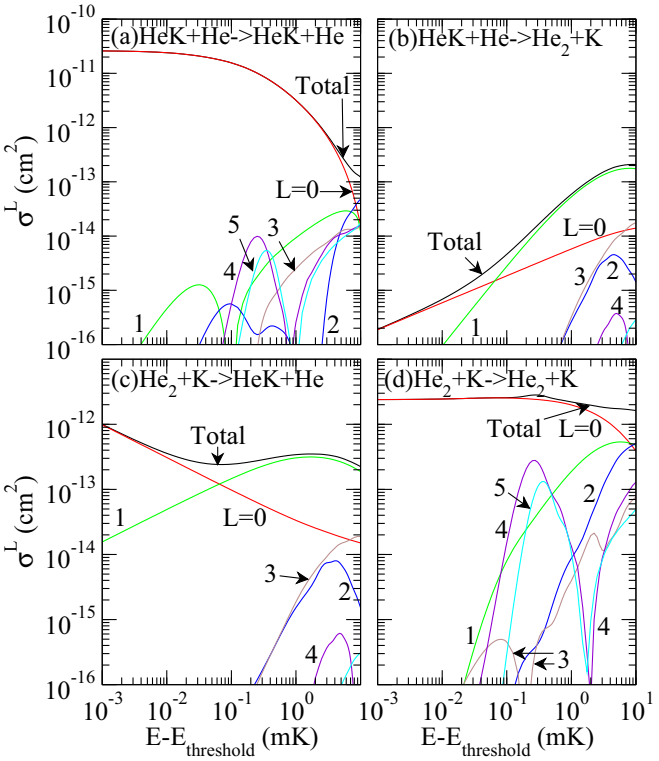

FIG. 3. (Color online) Total and partial cross sections for elastic and reactive atom-molecule collisions involving the ^{4}He-^{4}He-^{39}K system. We show cross sections for (a) $^4\mathrm{He}^{39}\mathrm{K} + {}^4\mathrm{He} \to {}^4\mathrm{He}^{39}\mathrm{K} + {}^4\mathrm{He}$, (b) $^4\mathrm{He}^{39}\mathrm{K} + {}^4\mathrm{He} \to {}^4\mathrm{He}_2 + {}^{39}\mathrm{K}$, (c) $^4\mathrm{He}_2 + {}^{39}\mathrm{K} \to {}^4\mathrm{He}^{39}\mathrm{K} + {}^4\mathrm{He}$, and (d) $^4\mathrm{He}_2 + {}^{39}\mathrm{K} \to {}^4\mathrm{He}_2 + {}^{39}\mathrm{K}$.

collision energies, the other partial cross sections are found to increase, and the convergence of the total cross section is not so certain. Like the elastic $^4He^7Li + ^4He$ collision process, the partial cross sections obey the Wigner threshold law $\sigma^L_{1\leftarrow 1} \sim (E - E_{00}^{^4He^4He})^{2L}$.

The total and partial cross sections for elastic and reactive collisions in the other ^{4}He–^{4}He–alkali-metal systems have been found to be mostly qualitatively similar to those in the ^{4}He-^{4}He-^{7}Li systems in the sense that, below some temperature, the $L = 0$ partial cross section dominates in the elastic collision processes and both $L = 0$ and $L = 1$ partial cross sections dominate in the reactive collisions. Here, we only present the results for the ^{4}He-^{4}He-^{39}K system in Figs. 3(a)–3(d) and for the ^{4}He-^{4}He-^{133}Cs system in Figs. 4(a)–4(d). For the elastic $^4He^{39}K + ^4He$ collision process in Fig. 3(a), the $L = 2$ partial cross section dominates at 10 mK, where the $L = 1$ partial-wave contribution happens to show a pronounced minimum. The $L = 3$–5 contributions are not as negligibly small either, compared to the $L = 0$–2 contributions. Clearly, the convergence of the total cross sections is uncertain at this collision energy. This is also the case for the elastic $^4He_2 + ^{39}K$ collision process. In addition, for the latter process, the $L = 4$ and 5 partial cross sections contribute to a certain extent around 0.1–0.2 mK, resulting in a hump in the energy dependency of the total cross section. For the ^{4}He-^{4}He-^{133}Cs system in Fig. 4, the total and partial cross sections behave in a qualitatively similar manner, and only the

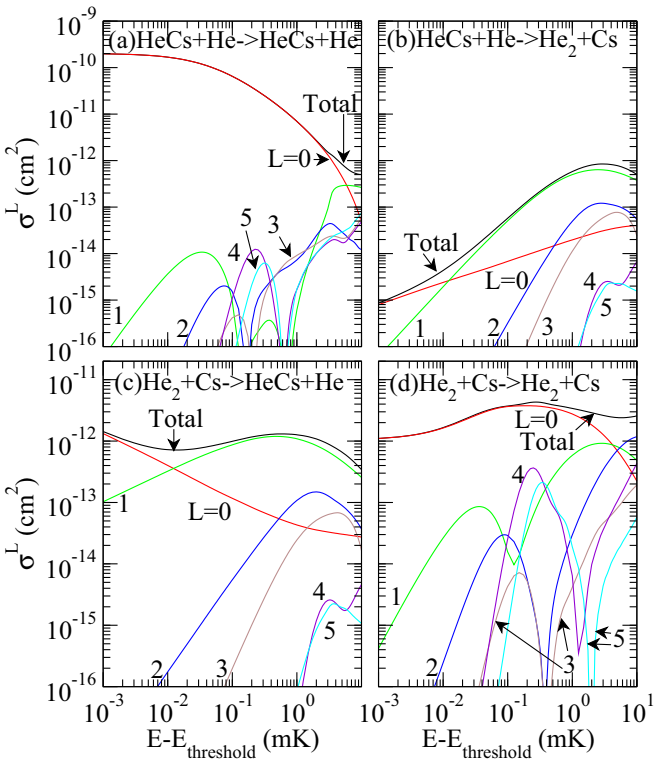

FIG. 4. (Color online) Total and partial cross sections for elastic and reactive atom-molecule collisions involving the ^{4}He-^{4}He-^{133}Cs system. We show cross sections for (a) $^4He^{133}Cs + ^4He \rightarrow ^4He^{133}Cs + ^4He$, (b) $^4He^{133}Cs + ^4He \rightarrow ^4He_2 + ^{133}Cs$, (c) $^4He_2 + ^{133}Cs \rightarrow ^4He^{133}Cs + ^4He$, and (d) $^4He_2 + ^{133}Cs \rightarrow ^4He_2 + ^{133}Cs$.

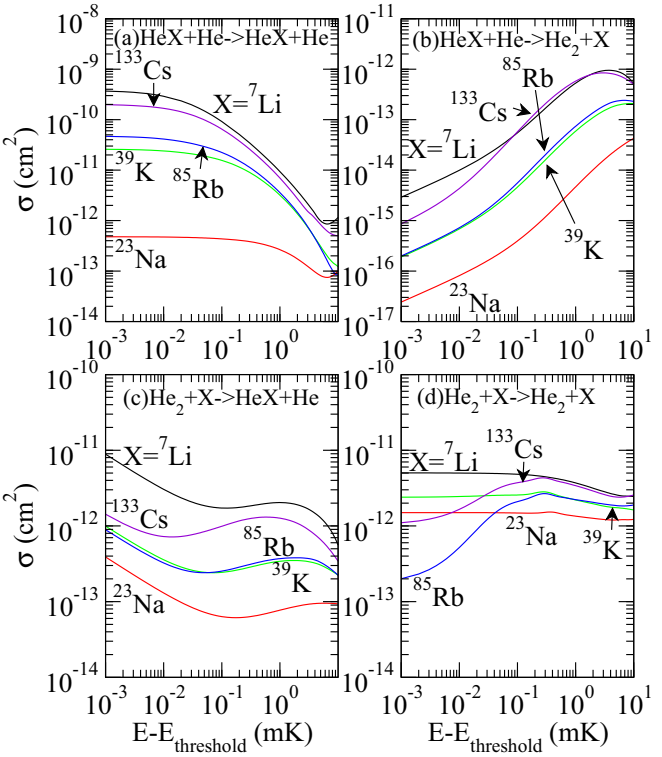

FIG. 5. (Color online) Total cross sections for elastic and reactive atom-molecule collisions involving ^{4}He-^{4}He-X systems with $X = ^7$Li, ^{23}Na, ^{39}K, ^{85}Rb, and ^{133}Cs. We show cross sections for (a) $^4HeX + ^4He \rightarrow ^4HeX + ^4He$, (b) $^4HeX + ^4He \rightarrow ^4He_2 + X$, (c) $^4He_2 + X \rightarrow ^4HeX + ^4He$, and (d) $^4He_2 + X \rightarrow ^4He_2 + X$.

increase in the total elastic $^4He_2 + ^{133}Cs$ cross section around the energies from 10^{-3} to 0.1 mK is a remarkable feature.

Finally, the total cross sections for all the collision processes considered in this work are summarized in Figs. 5(a)–5(d). For a given process, the total cross sections for different alkali-metal species are qualitatively similar to each other, while, for the elastic $^4He_2 + X$ process, we can see more similarity between $X = ^7$Li, ^{23}Na, and ^{39}K and between $X = ^{85}$Rb and ^{133}Cs. It is also notable that the total elastic $^4HeX + ^4He$ cross section at the zero-energy limit increases with the scattering length $a_{^4HeX}$ between ^{4}He and X, listed in Table I, implying that the zero-energy elastic $^4HeX + ^4He$ collision cross section is mainly determined by the size of the ^4HeX molecule. Moreover, the two reactive processes also seem to follow this trend. Only the elastic $^4He_2 + X$ cross section does not.

IV. SUMMARY

In this work, we have studied elastic and reactive atom-molecule collisions in ^{4}He–^{4}He–alkali-metal systems at cold collision energies. We have calculated the partial atom-molecule collision cross sections up to $L = 5$ relative angular momentum. In the ultracold limit, the elastic cross section is constant and the $L = 0$ partial wave dominates, while the reactive cross section behaves as either $(E - E_{00}^{^4He^4He})^{-1/2}$ or $(E - E_{00}^{^4He^4He})^{1/2}$, depending on whether the process is

exothermic or endothermic, respectively. As an extension of this work, the He + X + X systems are also interesting, but the large number of He + X_2 channels for alkali-metal atoms X currently poses technical difficulties.

ACKNOWLEDGMENTS

B.D.E. acknowledges support from the US National Science Foundation for the early stages of this work and from AFOSR-MURI for the later stages.

[1] C. Chin, R. Grimm, P. Julienne, and E. Tiesinga, Rev. Mod. Phys. **82**, 1225 (2010).
[2] Y. Wang, J. P. D'Incao, and B. D. Esry, Adv. Atom. Mol. Opt. Phys. **62**, 1 (2013).
[3] S. Jochim, M. Bartenstein, A. Altmeyer, G. Hendl, S. Riedl, and C. Chin, Science **302**, 2101 (2003).
[4] C. Chin, T. Kraemer, M. Mark, J. Herbig, P. Waldburger, H.-C. Nägerl, and R. Grimm, Phys. Rev. Lett. **94**, 123201 (2005).
[5] C. A. Regal, M. Greiner, and D. S. Jin, Phys. Rev. Lett. **92**, 040403 (2004).
[6] C. A. Stan, M. W. Zwierlein, C. H. Schunck, S. M. F. Raupach, and W. Ketterle, Phys. Rev. Lett. **93**, 143001 (2004).
[7] S. Inouye, J. Goldwin, M. L. Olsen, C. Ticknor, J. L. Bohn, and D. S. Jin, Phys. Rev. Lett. **93**, 183201 (2004).
[8] T. Weber, J. Herbig, M. Mark, H.-C. Nägerl, and R. Grimm, Phys. Rev. Lett. **91**, 123201 (2003).
[9] V. Efimov, Phys. Lett. B **33**, 563 (1970).
[10] E. Nielsen and J. H. Macek, Phys. Rev. Lett. **83**, 1566 (1999).
[11] B. D. Esry, C. H. Greene, and J. P. Burke, Jr., Phys. Rev. Lett. **83**, 1751 (1999).
[12] P. F. Bedaque, E. Braaten, and H.-W. Hammer, Phys. Rev. Lett. **85**, 908 (2000).
[13] E. Braaten and H.-W. Hammer, Phys. Rev. Lett. **87**, 160407 (2001).
[14] E. Braaten and H.-W. Hammer, Phys. Rep. **428**, 259 (2006).
[15] T. Kraemer, M. Mark, P. Waldburger, J. G. Danzl, C. Chin, B. Engeser, A. D. Lange, K. Pilch, A. Jaakkola, H.-C. Nägerl, and R. Grimm, Nature (London) **440**, 315 (2006).
[16] S. Knoop, F. Ferlaino, M. Mark, M. Berninger, H. Sch, H.-C. Nägerl, and R. Grimm, Nat. Phys. **5**, 227 (2009).
[17] T. B. Ottenstein, T. Lompe, M. Kohnen, A. N. Wenz, and S. Jochim, Phys. Rev. Lett. **101**, 203202 (2008).
[18] J. H. Huckans, J. R. Williams, E. L. Hazlett, R. W. Stites, and K. M. O'Hara, Phys. Rev. Lett. **102**, 165302 (2009).
[19] G. Barontini, C. Weber, F. Rabatti, J. Catani, G. Thalhammer, M. Inguscio, and F. Minardi, Phys. Rev. Lett. **103**, 043201 (2009).
[20] M. Zaccanti, B. Deissler, M. Fattori, M. Jona-Lasinio, M. I. G. Roati, and G. Modugno, Nat. Phys. **5**, 586 (2009).
[21] N. Gross, Z. Shotan, S. Kokkelmans, and L. Khaykovich, Phys. Rev. Lett. **103**, 163202 (2009).
[22] H. Suno, B. D. Esry, C. H. Greene, and J. P. Burke, Jr., Phys. Rev. A **65**, 042725 (2002).
[23] H. Suno and B. D. Esry, Phys. Rev. A **78**, 062701 (2008).
[24] Y. Wang, J. P. D'Incao, and B. D. Esry, Phys. Rev. A **83**, 032703 (2011).
[25] H. Suno and B. D. Esry, Phys. Rev. A **80**, 062702 (2009).
[26] H. Suno and B. D. Esry, Phys. Rev. A **82**, 062521 (2010).
[27] S. C. Doret, C. B. Connolly, W. Ketterle, and J. M. Doyle, Phys. Rev. Lett. **103**, 103005 (2009).
[28] W. Campbell and J. Doyle, in *Cold Molecules: Theory, Experiment, Applications* (Taylor and Francis, Boca Raton, FL, 2009), p. 473.
[29] N. Tariq, N. A. Taisan, V. Singh, and J. D. Weinstein, Phys. Rev. Lett. **110**, 153201 (2013).
[30] G. A. Parker, R. B. Walker, B. K. Kendrick, and R. T. Pack, J. Chem. Phys. **117**, 6083 (2002).
[31] J. Wang, J. P. D'Incao, and C. H. Greene, Phys. Rev. A **84**, 052721 (2011).
[32] M. Jeziorska, W. Cencek, B. Patkowsli, and K. Szalewicz, J. Chem. Phys. **127**, 124303 (2007).
[33] U. Kleinekathöfer, M. Lewerenz, and M. Mladenović, Phys. Rev. Lett. **83**, 4717 (1999).
[34] B. D. Esry, C. D. Lin, and C. H. Greene, Phys. Rev. A **54**, 394 (1996).
[35] C. D. Lin, Phys. Rep. **257**, 1 (1995).
[36] R. C. Whitten and F. T. Smith, J. Math. Phys. **9**, 1103 (1968).
[37] M. Aymar, C. H. Greene, and E. Luc-Koenig, Rev. Mod. Phys. **68**, 1015 (1996).
[38] J. P. Burke, Jr., Ph.D. thesis, University of Colorado, Boulder, 1999.
[39] B. Lepetit, Z. Peng, and A. Kuppermann, Chem. Phys. Lett. **166**, 572 (1990).
[40] B. K. Kendrick, R. T. Pack, R. B. Walker, and E. F. Hayes, J. Chem. Phys. **110**, 6673 (1999).
[41] C. de Boor, *A Practical Guide to Splines* (Springer, New York, 1978).